The Efimovian three-body potential from broad to narrow Feshbach resonances

The Efimovian three-body potential from broad to narrow Feshbach resonances

J. van de Kraats,[1,*] D.J.M. Ahmed-Braun,[1] J, -L. Li,[1,2] and S.J.J.M.F. Kokkelmans[1]

[1] *Eindhoven University of Technology, P. O. Box 513, 5600 MB Eindhoven, The Netherlands*
[2] *Institut für Quantenmaterie and Center for Integrated Quantum Science and Technology IQ ST , Universität Ulm, D-89069 Ulm, Germany*

(Dated: October 26, 2022)

We analyse the change in the hyperradial Efimovian three-body potential as the two-body interaction is tuned from the broad to narrow Feshbach resonance regime. Here, it is known from both theory and experiment that the three-body dissociation scattering length a_- shifts away from the universal value of $-9.7\ r_{\rm vdW}$, with $r_{\rm vdW} = \frac{1}{2}\left(mC_6/\hbar^2\right)^{1/4}$ the two-body van der Waals range. We model the three-body system using a separable two-body interaction that takes into account the full zero-energy behaviour of the multichannel wave function. We find that the short-range repulsive barrier in the three-body potential characteristic for single-channel models remains universal for narrow resonances, whilst the change in the three-body parameter originates from a strong decrease in the potential depth. From an analysis of the underlying spin structure we further attribute this behavior to the dominance of the two-body interaction in the resonant channel compared to other background interactions.

I. INTRODUCTION

In his seminal papers [1, 2], Vitaly Efimov predicted the appearance of an infinite and geometrically spaced set of three-particle bound states as the pairwise interaction becomes resonant. These Efimov states are bound by a universal attractive potential, decaying asymptotically as $-1/R^2$ for three particles at root mean square separation R. In trapped ultracold atomic gases the Efimov effect induces log-periodic peaks in the atom loss rate, driven by enhanced three-body recombination when an Efimov trimer crosses into the three-particle continuum [3–6]. The position of the loss peak associated with the ground state Efimov state sets a characteristic length scale a_-, commonly referred to as the three-body parameter. In three-body systems with zero-range interactions, introducing a three-body parameter is neccessary to regularise the scale invariant unbounded Efimov spectrum [5].

Despite its short-range nature, experiment has revealed that the three-body parameter in different atomic species attains a value close to $a_- = -9.7\ r_{\rm vdW}$ [7–11], where $r_{\rm vdW} = \frac{1}{2}\left(mC_6/\hbar^2\right)^{1/4}$ is the van der Waals length associated with the long-range two-body interaction. Subsequent theoretical studies have found that this "van der Waals universality" originates from a characteristic suppression of the two-body wave function when $r < r_{\rm vdW}$, where r is the two-particle separation [12, 13]. This suppression leads to the appearance of a strong repulsive barrier in the three-body potential at mean square separations $R \approx 2\ r_{\rm vdW}$, which shields the particles from probing the non-universal short-range detail of the atomic species.

The above-mentioned theoretical analyses are based on single-channel interaction potentials, which are expected to be accurate provided that the intrinsic length scale r_* due to the resonance width is much smaller than the potential range. This broad resonance regime may be defined by a large resonance strength parameter $s_{\rm res} = \bar{a}/r_* \gg 1$ [14], where $\bar{a} \approx 0.955978\ r_{\rm vdW}$ is the mean scattering length of the van der Waals interaction [15]. The opposite case of a narrow resonance, where $s_{\rm res} \ll 1$, is characterized by universal behaviour in terms of the dominant length scale $r_* \gg r_{\rm vdW}$. In this limit, treatments of the three-body problem which neglect the details of the van der Waals interaction have found the three-body parameter to be determined universally as $a_- = -10.9\ r_*$ [6, 16–18]. Connecting the broad and narrow resonance limits through the intermediate regime where $s_{\rm res} \approx 1$ with a van der Waals interaction model remains to be desired, in particular given that recent experiments in this regime in ^{39}K have revealed clear deviations from both universal limits [11]. A key aspect of this problem is the change in structure of the trimer and its associated potential energy surface as a function of the resonance strength, which will be the central topic of this paper.

In this work we study the Efimovian three-body potential using a realistic multichannel two-body van der Waals interaction, which can be easily tuned to probe a wide regime of resonance strengths. To solve the three-body problem we approximate this interaction by a separable potential which reproduces the zero-energy wave function of the original interaction. We then derive an effective three-body potential from the open-channel three-body wave function, which models the actual three-body potential that binds the Efimov state. Subsequently we study the dependence of this potential on the resonance strength $s_{\rm res}$, and provide an analysis of our findings in terms of the multichannel structure underlying the three-body dynamics.

This paper will be structured as follows. In Sec. II we outline our approach at the two-body level, first defining a two-channel model interaction with a Feshbach reso-

* j.v.d.kraats@tue.nl

nance that can be tuned from the broad to narrow resonance strength limit. Subsequently we formulate a separable approximation to this interaction. In Sec. III we move to the three-body level, which we analyse first in momentum space to facilitate our actual computations, and then subsequently in position space for our analysis of the three-body potential. In Sec. IV we present and analyse our results, after which we conclude this paper in Sec. V.

II. TWO-BODY INTERACTION MODELS

A. Model two-channel interaction

In this section we develop a flexible two-channel model that can be tuned to produce a Feshbach resonance with a given Breit-Wigner shape [19–21]. We define the Hamiltonian,

$$H(r) = \begin{pmatrix} -\frac{\hbar^2}{m}\nabla^2 + V_{\rm LJP}(r) & W(r) \\ W(r) & -\frac{\hbar^2}{m}\nabla^2 + V_{\rm LJP}(r) + \varepsilon_{\rm c}(B) \end{pmatrix}, \tag{1}$$

as a function of the two-body separation r and magnetic field B. The energy $\varepsilon_{\rm c}(B) > 0$ defines the energetic separation between the open and closed channels. We take the intrachannel interaction as the following van der Waals potential,

$$V_{\rm LJP}(r) = C_6 \left(\frac{r_0^4}{r^{10}} - \frac{1}{r^6} \right), \tag{2}$$

referred to as the Lennard-Jones-Pade (LJP) potential [22, 23]. By altering the short-range barrier length scale r_0 we tune $V_{\rm LJP}(r)$ such that it supports 8 dimer states. We have confirmed that with this choice the three-body parameter in the broad resonance limit has converged to the universal van der Waals value.

A Feshbach resonance is induced when a closed-channel bound state becomes degenerate with the open-channel threshold energy. Inspired by Ref. [19], we take the resonant state to be the second bound state in the LJP potential, as counted from the threshold energy. In the absence of coupling, the bound state with negative energy $-\varepsilon_{\rm b}$ relative to threshold will become resonant with the open-channel if $\varepsilon_{\rm c}(B_{\rm res}) = \varepsilon_{\rm b}$. If the magnetic field is tuned away from $B_{\rm res}$ the bound state shifts linearly in accordance with the open-closed channel magnetic moment difference $\delta\mu$ [14]. Thus,

$$\varepsilon_{\rm c}(B) = \varepsilon_{\rm b} + \delta\mu\,(B - B_{\rm res})\,. \tag{3}$$

The off-diagonal couplings $W(r)$ shift the bare resonant magnetic field $B_{\rm res}$ to the dressed resonant value B_0. On resonance, the s-wave scattering length diverges, parametrised by the relation [14],

$$a(B) = a_{\rm bg}\left(1 - \frac{\Delta B}{B - B_0}\right). \tag{4}$$

Here $a_{\rm bg}$ is the background scattering length in the open-channel potential. We model the coupling by a Gaussian potential, also used in Ref. [21],

$$W(r) = \beta e^{-\alpha(r - r_W)^2}. \tag{5}$$

The coupling parameters α, β and r_W may be tuned to produce a certain magnetic field width,

$$\Delta B \underset{k\to 0}{=} \frac{\pi}{a_{\rm bg} k \delta\mu} |\,\langle \phi_{\rm res}|W|\psi_\varepsilon\rangle|^2. \tag{6}$$

Here $|\phi_{\rm res}\rangle$ is the unit normalised wave function of the resonant bound state, $|\psi_\varepsilon\rangle$ is the energy normalised scattering wave function in the open-channel, and $k = \sqrt{m\varepsilon/\hbar^2}$. To simplify our approach we have elected to fix $r_W = 0.15\ r_{\rm vdW}$ [24]. In van der Waals potentials it is possible to approximate B_0 using the techniques of multichannel quantum defect theory (MQDT) [25–29]. This leads to the direct relation,

$$B_0 = B_{\rm res} + \left[\frac{r_{\rm bg}(1 - r_{\rm bg})}{1 + (1 - r_{\rm bg})^2}\right]\Delta B, \tag{7}$$

where $r_{\rm bg} = a_{\rm bg}/\bar{a}$.

The two-channel model outlined in this section takes a set of experimental resonance parameters $\{a_{\rm bg}, \Delta B, B_0\}$ as input. Then the equations derived above map these to a set of model parameters $\{r_0, \alpha, \beta, B_{\rm res}\}$, which subsequently fix the Hamiltonian H. The resulting resonance strength is then obtained as [14],

$$s_{\rm res} = \frac{m}{\hbar^2}\bar{a} a_{\rm bg} \delta\mu \Delta B, \tag{8}$$

which quantifies the ratio $r_*/\bar{a}$ as mentioned in Sec. I.

B. EST separable potential

As pointed out in previous studies, the universal van der Waals three-body parameter and three-body potential can be reproduced by accounting for the full finite-range detail of the van der Waals interaction [12]. Similarly it was recently shown that reproducing the three-body recombination rate for resonances of intermediate strength in ^{39}K requires an inclusion of the exact three-body spin structure in the Hamiltonian [30]. Such approaches however, are complicated numerically, and not conducive to our goal of developing a simple and flexible model. Fortunately it was pointed out in Refs. [13, 31] that van der Waals universality can be reproduced using a much simpler model, based on the Ernst, Shakin and Thaler (EST) separable potential [32]. In this section we develop such an approach for our multichannel interaction. The crucial point is that we approximate the interaction in such a way that the full two-body wave function at zero energy is taken into account, whilst retaining the simplicity of a single-term separable potential.

We define $V(r)$ as the part of $H(r)$ that vanishes as $r \to \infty$. The associated operator is approximated using a separable interaction $V^{\rm sep}$, defined as,

$$V^{\rm sep} = |g\rangle\, \xi\, \langle g|\,. \tag{9}$$

The states $|g\rangle$ are referred to as the form factors of the potential. Given an exact eigenstate $|\psi\rangle$ of the Hamiltonian H, we define the separable potential as,

$$|g\rangle = V\,|\psi\rangle\,, \qquad \xi^{-1} = \langle\psi|V|\psi\rangle\,. \tag{10}$$

With these definitions one may show that $|\psi\rangle$ is also an eigenfunction of the Hamiltonian where V is replaced with $V^{\rm sep}$, with the exact same eigenvalue [32]. Similar to Ref. [13], we take $|\psi\rangle$ to be the zero-energy scattering state, such that our model takes as input the low-energy scattering detail of the actual interaction. The separable interaction has an associated separable t-matrix, given by the Lipmann-Schwinger equation [33],

$$t^{\rm sep}(z) = V^{\rm sep} + V^{\rm sep} G_0(z) t^{\rm sep}(z). \tag{11}$$

Here $G_0(z) = (z - H_0)^{-1}$ is the Green's function associated with the free Hamiltonian $H_0 = H - V$. We define its s-wave eigenstates as $|k, \sigma\rangle$, where $k = |\mathbf{k}|$ is the relative momentum and $\sigma = \{1, 2\}$ the scattering channel with associated two-body energy ε_σ at infinite separation. We always assume that only the lowest channel $\sigma = 1$ is energetically open. Expressed in this basis we obtain,

$$t^{\rm sep}_{\sigma',\sigma}(z, k', k) = g_{\sigma'}(k')\tau(z) g^*_\sigma(k), \tag{12}$$

where $t^{\rm sep}_{\sigma',\sigma}(z, k', k) = \langle k', \sigma'|t^{\rm sep}(z)|k, \sigma\rangle$ and $g_\sigma(k) = \langle k, \sigma|g\rangle$. The function $\tau(z)$ is given by,

$$\tau^{-1}(z) = \frac{m}{\hbar^2}\left[\frac{2\pi^2}{a}|g_1(0)|^2 + 4\pi \sum_\sigma \int_0^\infty dk \frac{k^2 \left(\frac{mz}{\hbar^2}\right)|g_\sigma(k)|^2}{\left(k^2 + \frac{m\varepsilon_\sigma}{\hbar^2}\right)\left(k^2 + \frac{m\varepsilon_\sigma}{\hbar^2} - \frac{mz}{\hbar^2}\right)}\right], \tag{13}$$

for particle mass m and open channel form factor $g_1(k)$. This form is inspired by Ref. [6], and uses the fact that the zero-energy on-shell transition matrix is related to the scattering length as $t_{1,1}(0, 0, 0) = \hbar^2 a/(2\pi^2 m)$. The form factors can be computed directly from Eq. (10), by inserting complete sets of position states. Our normalisation gives $\langle \mathbf{r}|k, \sigma\rangle \sim \sin(kr)/(kr)\,|\sigma\rangle$, and we expand the scattering wavefunction into channel functions $u_\sigma(r)$ as,

$$\langle \mathbf{r}|\psi\rangle \sim \sum_\sigma \frac{u_\sigma(r)}{r}\,|\sigma\rangle\,. \tag{14}$$

Then the form factors, normalised such that $g_1(0) = 1$, are given by,

$$g_\sigma(k) = \frac{\sum_{\sigma'} \int_0^\infty dr\ \sin(kr)\ V_{\sigma,\sigma'}(r)\ u_{\sigma'}(r)}{k \sum_{\sigma'} \int_0^\infty dr\ r\ V_{1,\sigma'}(r)\ u_{\sigma'}(r)}, \tag{15}$$

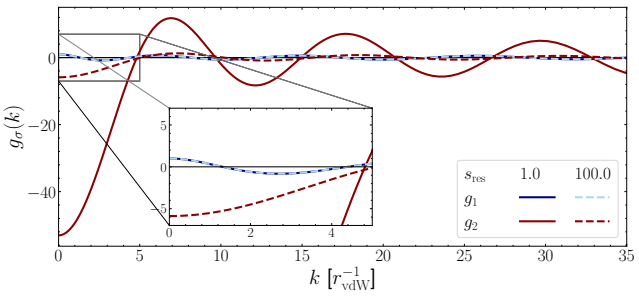

FIG. 1. The form factors $g_\sigma(k)$ as a function of momentum k, tuned to two different resonance strengths. Inset shows a zoom of the low momentum regime, where one observes the normalisation $g_{\rm o}(0) = 1$.

where $V_{\sigma,\sigma'} = \langle\sigma|V|\sigma'\rangle$. To illustrate the EST potential we plot the functions $g_\sigma(k)$ in Fig. 1, using as input the two-channel model from the previous section tuned to a broad and intermediate resonance strength. Since the open-channel component of the wave function is independent of $s_{\rm res}$ (see Sec. IV B), the open-channel form factors are much less sensitive to changes in the resonance strength than the closed-channel form factors.

Note that the EST model as developed here straightforwardly simplifies in the case of a single-channel interaction (broad resonance limit), where one will need just a single radial wave function as input. For single-channel interactions we evaluate the radial Schrödinger equation using the potential following Numerov method [34], whilst we apply a mapped grid DVR method in the multichannel case [35, 36]. We emphasize that the EST model is based on the zero-energy wave function, and hence loses accuracy when used to describe deep bound states. To illustrate this behaviour we have computed the shallow dimer energy around the 8th potential resonance in the two-channel model, both by a direct numerical solution of the multichannel Schrödinger equation, and via the EST potential of this section. In the latter case a dimer solution is found through the condition $\tau^{-1}(\varepsilon) = 0$, with $\varepsilon < 0$ the binding energy. The two results are compared in Fig. 2, where one observes that the EST potential is most accurate near threshold, and is thus naturally suited to treat states near resonance. For smaller scattering lengths the EST potential becomes inaccurate for the broad resonance where the dimer becomes too strongly bound, but remains reasonably accurate in describing narrower resonances. In this paper we only concern ourselves with the near resonant regime $a \gg r_{\rm vdW}$, where the EST potential is accurate regardless of the resonance strength. Finally, while we will limit ourselves to the two-channel interaction of Sec. II A, the EST potential as developed here can take any multichannel interaction as input. This means that next to simple model two-channel interactions one could also use more realistic molecular potentials with many spin-channels. In Appendix C, we apply this method to analyse a Feshbach resonance in ^{39}K, and subsequently compare the

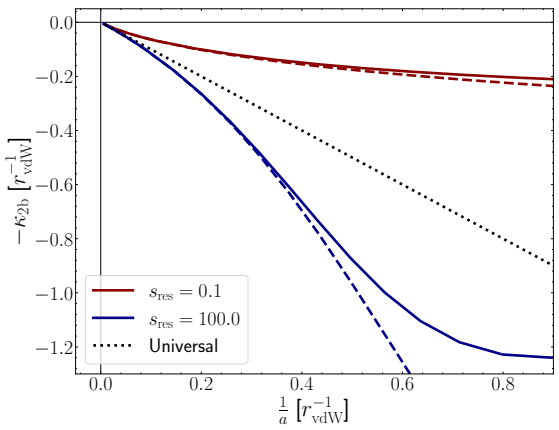

FIG. 2. Binding wavenumber $\kappa_{2b} = \sqrt{m|\varepsilon|\,/\hbar^2}$ of the Feshbach dimer that manifests in the two-channel model of Sec. II A, as a function of inverse scattering length. Results are shown both with the EST model potential (solid lines), and a direct solution of the multichannel Schrödinger equation (dotted lines). We show results for two different resonance strengths, and additionally plot the universal resonant result $\kappa_{2b} \sim 1/a$.

obtained three-body parameter to experiment.

III. THREE-BODY APPROACH

A. The ESC-EST model

At the three-body level we formulate what will henceforth be referred to as an effective single-channel (ESC) model. In this approach we only include the influence of the closed channel on the shape of the two-body t-matrix, neglecting the multichannel structure on the three-body level. This approximation significantly simplifies the model whilst retaining the characteristic change in three-body parameter near narrow resonance [18]. We start by writing the momentum-space three-body wavefunction $\Psi(\mathbf{k},\mathbf{p})$ of the bound-state into the Faddeev decomposition [37],

$$\Psi(\mathbf{k},\mathbf{p}) = (1 + P_+ + P_-)\,\bar{\Psi}(k,p), \tag{16}$$

where $P_{+/-}$ are cyclic/anticyclic permutation operators of the particle indices, $\{k,p\}$ are the dimer and atom-dimer Jacobi momenta respectively, and $\bar{\Psi}(k,p) \equiv \langle k,p|\bar{\Psi}\rangle$ is the s-wave Faddeev component. For a three-body bound state with energy $E<0$ the Faddeev component is determined by the following integral equation [38, 39]

$$\begin{aligned}\bar{\Psi}(k,p) = 2\int d^3\mathbf{q}\,\left[E - \frac{3}{4}\frac{\hbar^2p^2}{m} - \frac{\hbar^2k^2}{m}\right]^{-1} \\ t\left(E - \frac{3}{4}\frac{\hbar^2p^2}{m}, k, \left|\mathbf{q}+\frac{\mathbf{p}}{2}\right|\right)\bar{\Psi}\left(\left|\mathbf{p}+\frac{\mathbf{q}}{2}\right|, q\right).\end{aligned} \tag{17}$$

Here $t(z,k,p)$ is the single-channel s-wave two-body transition matrix. In the ESC-EST model we take this equation and make the replacement $t \to t^{\rm sep}_{1,1}$, i.e. we insert the open-channel component of the separable transition matrix into the single-channel three-body equations. We shall discuss the assumptions on the three-body spin-structure inherent to this approach in more detail in Sec. IV C. To model the $s_{\rm res} \gg 1$ broad resonance limit we additionally introduce a "bare" single-channel (SC) model. Here the closed-channel is completely eliminated and the Efimov effect is induced via a potential resonance in the interaction potential. This SC-EST model is equivalent to the approach taken in Refs. [13, 31, 40].

Going forward we write the three-body bound state energy in terms of a wavenumber $\kappa = \sqrt{m|E|/\hbar^2}$. Upon substitution of the separable transition matrix as defined by Eqs. (12, 13) in Eq. (17) the Faddeev component can be computed as,

$$\bar{\Psi}(k,p) = -\frac{F(\kappa,p)g_1(k)}{\frac{3}{4}p^2 + k^2 + \kappa^2}. \tag{18}$$

Here the function $F(\kappa,p)$ is given by the Skorniakov-Ter-Martirosian (STM) equations [41],

$$\tau^{-1}\left(Z(\kappa,p)\right)F(\kappa,p) + 2\int d^3\mathbf{q}\;\mathcal{Z}(\kappa,\mathbf{p},\mathbf{q})F(\kappa,q) = 0, \tag{19}$$

with $mZ(\kappa,p)/\hbar^2 = -\kappa^2 - 3p^2/4$ and,

$$\mathcal{Z}(\kappa,\mathbf{p},\mathbf{q}) = \frac{g_1^*\left(|\mathbf{q}+\frac{1}{2}\mathbf{p}|\right)g_1\left(|\frac{1}{2}\mathbf{q}+\mathbf{p}|\right)}{p^2+q^2+\mathbf{p}\cdot\mathbf{q}+\kappa^2}. \tag{20}$$

Upon discretization on a momentum grid the STM equations become matrix equations which can be solved to obtain the three-body wavenumber κ and the Faddeev component $\bar{\Psi}(k,p)$.

B. Effective three-body potential

The momentum space approach as outlined in the previous section will be used for our numerical computations. However, for the analysis of the Efimovian three-body potential, we need to make a transformation to position space. In this section we give a brief overview of the hyperspherical formalism in which the Efimovian potential is usually expressed. For a more detailed discussion of the formulation we refer to Refs. [5, 42–44].

For identical particles, the Jacobi dimer separation r_i and atom-dimer separation ρ_i are transformed to a hyperradius R and hyperangle α_i,

$$\tan\alpha_i = \frac{\sqrt{3}r_i}{2\rho_i}, \quad R^2 = r_i^2 + \frac{4}{3}\rho_i^2, \tag{21}$$

Here $i = 1,2,3$ denotes the Jacobi index, which we will suppress in this section. As the notation implies, R is

invariant to a change in Jacobi set. The hyperangle α is often denoted together with the polar and azimuthal angles of the unit vectors $\hat{\mathbf{r}}$ and $\hat{\boldsymbol{\rho}}$ as $\boldsymbol{\Omega}$. The three-body wavefunction in these coordinates may be expanded into a complete and orthonormal set of *hyperangular functions* $\Phi_\nu(R,\boldsymbol{\Omega})$, by the following expansion,

$$\Psi(R,\boldsymbol{\Omega}) = \frac{1}{R^{\frac{5}{2}}}\sum_{\nu=0}^{\infty} f_\nu(R)\Phi_\nu(R,\boldsymbol{\Omega}). \tag{22}$$

The hyperangular functions $\Phi_\nu(R,\boldsymbol{\Omega})$ are eigenfunctions of the angular momentum part of the three-body Schrödinger equation. The index ν is usually referred to as the hyperspherical channel, and the associated expansion coefficient $f_\nu(R)$ as the hyperradial wave function. It obeys the following set of coupled equations [45],

$$\begin{aligned}&\left[-\frac{\mathrm{d}^2}{\mathrm{d}R^2} + \frac{\lambda_\nu(R)-\frac{1}{4}}{R^2} + \kappa^2 + Q_{\nu\nu}(R)\right] f_\nu(R)\\ &+\sum_{\nu'\neq\nu}\left[Q_{\nu\nu'}(R) + 2P_{\nu\nu'}(R)\frac{\mathrm{d}}{\mathrm{d}R}\right] f_{\nu'}(R) = 0.\end{aligned} \tag{23}$$

Here $\lambda_\nu(R)$ is the eigenvalue associated with the hyperangular function $\Phi_\nu(R,\boldsymbol{\Omega})$, where R is interpreted as a parameter of the eigenvalue equation. Eq. (23) defines an infinite set of equations coupled through the presence of the coupling potentials,

$$\begin{aligned}P_{\nu\nu'}(R) &= -\langle\Phi_\nu|\frac{\partial}{\partial R}|\Phi_{\nu'}\rangle_{\boldsymbol{\Omega}},\\ &\text{and}\\ Q_{\nu\nu'}(R) &= -\langle\Phi_\nu|\frac{\partial^2}{\partial R^2}|\Phi_{\nu'}\rangle_{\boldsymbol{\Omega}}.\end{aligned} \tag{24}$$

The inner products on the right-hand side should be taken over the space of angular coordinates $\boldsymbol{\Omega}$. The coupling potentials quantify the dependence of the hyperangular distribution on the hyperradius, and are often referred to as non-adiabatic contributions to the three-body problem [45]. In the so called *scale-free* region, where $r_{\mathrm{vdW}} \ll R \ll |a|$, one may show that the eigenvalue λ becomes independent of the hyperradius [5]. This has the consequence that all non-adiabatic contributions vanish and the coupled set presented in Eq. (23) uncouples into single particle Schrödinger equations with "effective" hyperradial three-body potentials $U_m(R) = (\lambda_\nu - \frac{1}{4})/R^2$. The Efimov channel $\nu = 0$ has eigenvalue $\lambda_0 = -s_0^2$, with $s_0 \approx 1.00624$. Thus the associated three-body potential is attractive, inducing the Efimov effect with its characteristic $1/R^2$ scaling. In the scale-free region all channels with $\nu \neq 0$ have associated three-body potentials that are purely repulsive [45].

Due to the non-trivial behaviour of the coupling potentials in the short-range regime, the full behaviour of the effective potential is very complicated. Upon solving the STM equation (19) however, we can use the three-body wave function to derive an approximation to the Efimovian three-body potential. First we formulate the three-body probability as,

$$\bar{P}_{\boldsymbol{\Omega}}(R) \sim R^5\int_0^{\frac{\pi}{2}} d\alpha\ \sin^2(2\alpha)\int_{-1}^{1} dx\ |\Psi(R,\alpha,x)|^2, \tag{25}$$

where $\Psi(R,\alpha,x)$ is obtained by a Fourier transformation of Eq. (16). By virtue of the orthonormality of the hyperangular functions $\Phi(R,\boldsymbol{\Omega})$ it is possible to use the three-body probability to derive an *effective* three-body potential, a method also applied in Ref. [13]. The validity of this method relies on the efficiency of the hyperspherical expansion in Eq. (22). In the scale-free region the Efimov channel is the only attractive channel, such that we are justified in neglecting all higher lying repulsive channels which suppress the local probability [12]. Then the expansion contains only one term, and the resulting three-body probability is equal to $|f_0(R)|^2$. Since we can choose $f_0(R)$ to be real by the normalisation of the wave function, the following expression for an effective three-body potential follows from Eq. (23),

$$U_{\mathrm{eff}}(R) = \frac{1}{\sqrt{\bar{P}_{\boldsymbol{\Omega}}(R)}}\frac{\mathrm{d}^2}{\mathrm{d}R^2}\sqrt{\bar{P}_{\boldsymbol{\Omega}}(R)} - \kappa^2. \tag{26}$$

At unitarity this effective potential is expected to be a good approximation of the actual Efimov potential, provided that the hyperradius not be too small such that coupling to higher lying channels is negligible. In particular it is sufficiently accurate to reproduce the characteristic repulsive barrier around $R \approx 2\ r_{\mathrm{vdW}}$ and the potential well which appear for broad resonances, as was shown in Ref. [13].

TABLE I. Parameters of the physical resonances used as a starting point for our computations. The value of s_{res} in the last column will be varied with all other parameters held fixed. Data taken from (^{39}K: [46]), (^{85}Rb: [47, 48]) and (^{133}Cs: [14, 49]).

Species	B_0 [G]	a_{bg} [r_{vdW}]	$\delta\mu$ [E_{vdW}/G]	s_{res}
^{39}K	33.50	-0.31	-0.154	2.46
^{85}Rb	155.04	-5.40	-0.517	28.6
^{133}Cs	-11.7	17.02	1.21	565
^{133}Cs	547.0	24.74	0.94	167

IV. RESULTS

To fix the degrees of freedom in the model of Sec. II A we take sets of resonance parameter measured from physical resonances, summarised in table I. We then shift the resonance strength s_{res} away from the physical value by altering ΔB, keeping all other parameters fixed. As reported in Ref. [50], the change in the three-body parameter with varying resonance strength becomes more

abrupt as $a_{\rm bg}$ approaches the value of a_- in the open-channel potential. We check whether our model reproduces this behaviour by artifically altering the Rubidium resonance such that $a_{\rm bg} = -9.75\ r_{\rm vdW}$, noting that the open-channel LJP potential has a three-body parameter $a_- = -10.85\ r_{\rm vdW}$ in the EST approximation.

A. Efimov spectra

We first apply our model to the computation of the Efimov spectra and associated three-body parameters as a function of the Feshbach resonance strength. First, we show in Fig. 3 the spectrum of the two lowest lying Efimov states for finite scattering lengths surrounding the Feshbach resonance. Comparing with the broad resonant limit $s_{\rm res} \to \infty$, we find that as the resonance strength is decreased the Efimov spectrum is squeezed into a smaller area of the $(\kappa, 1/a)$ plane, corresponding to an increase of the three-body parameter $|a_-|$. Alternatively one can also define the three-body parameter via the wavenumber κ_* of the ground state trimer at resonance, which decreases as the resonance becomes narrow.

The shift in three-body parameters can be more clearly seen in Fig. 4, where we show a scan of $|a_-|$ and κ_* from the broad to narrow resonance limit. For the sake of comparison, Fig. 4 also contains experimental data for a select set of physical resonances. As the resonance strength decreases, the three-body parameter $|a_-|$ shows a monotonous increase, consistent with findings in earlier studies such as Refs. [50, 51], but inconsistent with the findings of Ref. [52] which finds the reverse behaviour. Consequently we obtain a better match with the experimental data for ^{39}K than for ^{7}Li, which similarly trends to smaller values of $|a_-|$ for decreasing $s_{\rm res}$. Recent work has shown that both an increasing and decreasing $|a_-|$ may be obtained by including the multichannel structure in the three-body equations [18], which by definition is neglected in the ESC model. Within the narrow resonance limit our results approach the universal limit $a_- = -10.9\ r_*$. The effect of the background scattering length can mainly be observed in the intermediate strength regime, where larger negative values of $a_{\rm bg}$ tend to push the three-body parameter closer to the universal broad resonance value for a larger portion of the resonance strength regime. This finding is consistent with more artificial models of the two-body interaction such as the approach adopted in Ref. [50]. However, our more realistic EST model strongly suppresses the sensitivity of the three-body parameter to the background scattering length. This is especially true for the binding wave number κ_*, whose dependence on $a_{\rm bg}$ is negligible on the scale of Fig. 4. This behaviour shows some correspondence with the effective range in multichannel van der Waals potentials, which also becomes independent of $a_{\rm bg}$ on resonance [53]. Hence any $a_{\rm bg}$ dependence originates from higher order terms in the effective range expansion, which are seemingly small in our model [50]. To verify

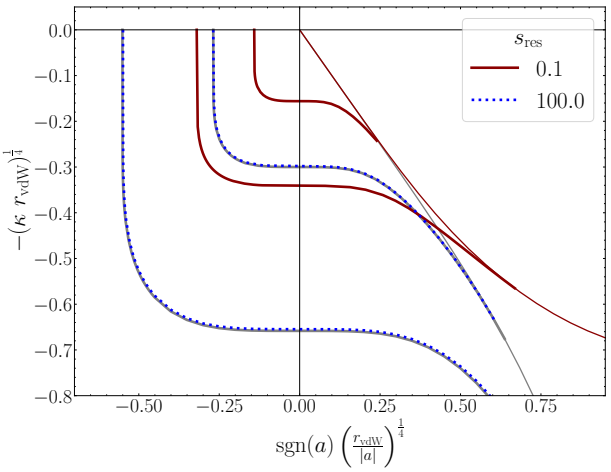

FIG. 3. Binding wave number of the two lowest lying Efimov states as a function of the inverse scattering length, computed at two different resonance strengths. For $a > 0$ the atom-dimer thresholds from Fig. 2 are plotted with thin lines. Grey lines show the energies obtained from a single-channel SC-EST model, which corresponds with the broad-resonance limit $s_{\rm res} \to \infty$.

that a strong $a_{\rm bg}$ dependence is inherent to more artificial interaction potentials we have compared our results to three-body parameters obtained from a constant interaction with a simple ultraviolet cut-off. The results are presented in Appendix D.

B. Three-body repulsion

Having confirmed that the three-body parameter in our model scales as expected in both the narrow and broad resonance limits, we now move on to a position space analysis using the formalism of Sec. III B. Given that our results are largely insensitive to $a_{\rm bg}$ at the position of the resonance, we limit ourselves in this section to the ^{39}K resonance with $a_{\rm bg} = -0.31\ r_{\rm vdW}$. Before analyzing the three-body state directly it is instructive to consider the two-body scattering wave function $\langle r|\psi\rangle$ of Eq. (14) that is used to construct the EST potential. To this end we plot the open and closed channel radial components of the wave function for a set of different resonance strengths in Fig. 5, normalised such that the wave function asymptotes to 1 for $r \gg r_{\rm vdW}$. As predicted by multichannel resonance theory the open-channel amplitude $|u_1(r)|$ is $s_{\rm res}$ independent, whilst the closed-channel amplitude $|u_2(r)|$ scales as $\sim 1/\sqrt{s_{\rm res}}$ [55]. Previous analyses of single-channel van der Waals interactions have connected the suppression of the two-body wave function below distances of 1 $r_{\rm vdW}$ to the appearance of a universal repulsive barrier in the three-body potential at $R \approx 2\ r_{\rm vdW}$ [12, 13]. In the two-channel case this suppression persists in the open-channel component, whilst there appears an increase in total short-

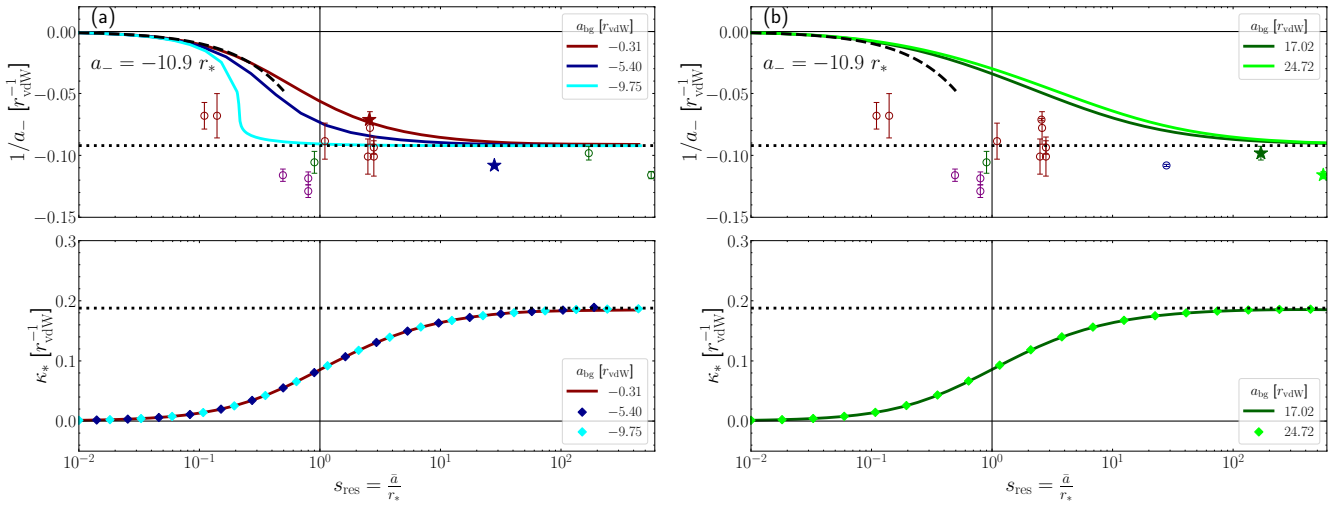

(a) (b)

FIG. 4. Plots of the three-body parameters as a function of resonance strength, for negative $a_{\rm bg}$ in Fig. (a) and positive $a_{\rm bg}$ in Fig. (b). In the top panels we show the inverse of the dissociation scattering length a_- associated with the ground state Efimov trimer. Here solid coloured lines show the results of the ESC-EST model, for different background scattering lengths. Scatter points represent experimental data, measured in ^{133}Cs (green) [7], ^{7}Li (purple) [8, 9], ^{85}Rb (dark blue) [10] and ^{39}K (dark red) [11, 54]. The colour of the line plots is chosen to match the data points, e.g. the red plots were computed using resonance parameters matching a resonance in ^{39}K . Experimental data obtained for specific resonances taken as starting points for the ESC-EST model (see table I), are shown as a star in the appropriate colour. In the narrow resonance limit $s_{\rm res} \ll 1$ we illustrate the limiting behaviour $a_- = -10.9\ r_*$ as a thick black dashed line. In the bottom panels we plot the trimer binding wavenumber κ_* at resonance. Here, results for different background scattering length practically overlap on the scale shown here, so we use scatter plots to distinguish between them. In both the upper and lower panels the three-body parameter obtained with a single-channel EST model, correspondent with the broad resonance limit $s_{\rm res} \gg 1$, is shown as a black dotted line.

range two-body probability due to finite lifetime of the closed-channel state.

To examine the effect of the closed-channel on the three-body level we first compute the three-body probability in the $\{R, \alpha\}$ plane, by omitting the integration over the hyperangle in Eq. (25). The results are shown in Fig. 6. Here the effect of the open-channel suppression is highlighted by plotting the boundary beyond which any two particles approach below the van der Waals length. As expected, the three-body probability is strongly suppressed beyond this boundary for the broad resonance (first two panels of Fig. 6), where the closed-channel component is small. Interestingly, as we tune our interaction towards the narrow resonance regime and the closed-channel amplitude increases we see no additional penetration of the region of open-channel suppression. Instead, we find that both the average and the spread of the three-body wave function in the hyperradial coordinate increase. This suggests that the open-channel suppression of two-body probability remains a dominant factor for small hyperradii, strongly suppressing the three-body probability regardless of resonance strength. The increase in closed-channel two-body amplitude mainly impacts the intermediate to long distance regime where $R > 2\ r_{\rm vdW}$. As has been noted before [12, 13], the appearance of a three-body repulsive barrier is associated with a repulsive potential energy peak due to the non-adiabatic correction $Q_{00}(R)$ in Eq. (23), reminiscent of an angular momentum barrier. This peak arises due to a squeezing of the hyperangular distribution function $\Phi(R, \mathbf{\Omega})$ as R decreases, driven by the short-range two-body suppression. Our results in Fig. 6 show that the location of this barrier remains universally determined by the van der Waals length also near a narrow resonance.

We now proceed by integrating out the hyperangle to obtain $\bar{P}_{\mathbf{\Omega}}(R)$ and use Eq. (26) to derive the effective three-body potential. The results are plotted in Fig. 7, where for the sake of comparison we also show the result with a single-channel interaction (correspondent with $s_{\rm res} \to \infty$), and the universal $\sim 1/R^2$ potential from zero-range theory giving the limit $R/r_{\rm vdW} \to \infty$ [5]. Consistent with Fig. 6, a decreasing resonance strength manifests most strongly in the intermediate to long distance regime, where we observe a strong decrease in the depth of the effective potential that pushes the Efimov state closer to threshold. This is consistent with a decrease of the binding energy κ_* as noted in Fig. 4. To verify whether this behaviour continues into the narrow resonance limit, we have tracked the effective potential up to $s_{\rm res} = 0.01$. Here the potential at larger separations becomes practically flat, signifying that all hyperradii have approximately equal probability. To obtain a more quan-

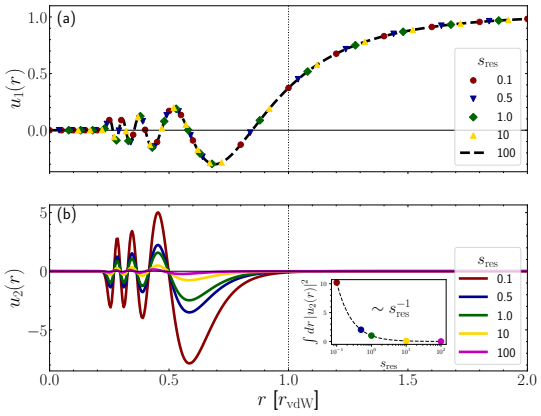

FIG. 5. Open (a) and closed (b) channel functions $u_1(r)$ and $u_2(r)$ for different values of the resonance strength, computed at unitarity for the Feshbach resonance with $a_{\rm bg} = -0.31\ r_{\rm vdW}$. The $r = r_{\rm vdW}$ boundary is emphasized by the black dotted line. The normalisation is chosen such that the total wave function asymptotes to unity in the long range. The inset in figure (b) shows the scaling of the integrated closed-channel two-body probability with $s_{\rm res}$.

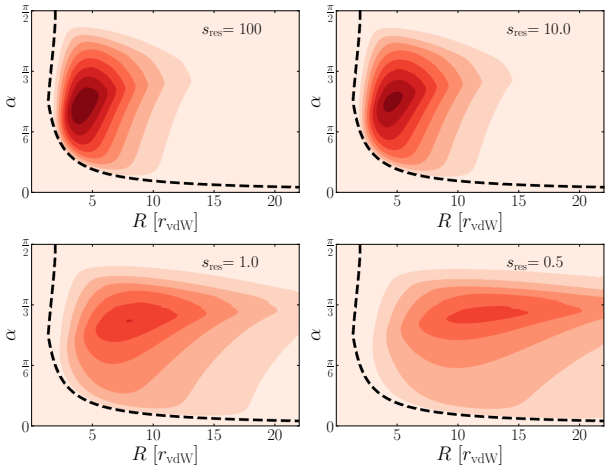

FIG. 6. Contour plots of the three-body probability at four different values of $s_{\rm res}$. Computed using the ^{39}K resonance with $a_{\rm bg} = -0.31\ r_{\rm vdW}$ as input. The boundary below which any two particles approach closer than 1 $r_{\rm vdW}$ is shown by a black dashed line. Format inspired by Ref. [13]

titative characterisation of the decrease in depth we plot the minimum of the effective potential as a function of $s_{\rm res}$, shown in the inset of Fig. 7. In the broad resonance limit we find that the depth of the barrier scales with $1/\sqrt{s_{\rm res}}$, and is hence inversely proportional to the closed-channel amplitude as plotted in Fig. 5. Consistent with Fig. 6 the position of the repulsive barrier is set by the van der Waals length with the relation $R \approx 2\ r_{\rm vdW}$, regardless of the resonance strength.

To supplement our findings we have also computed

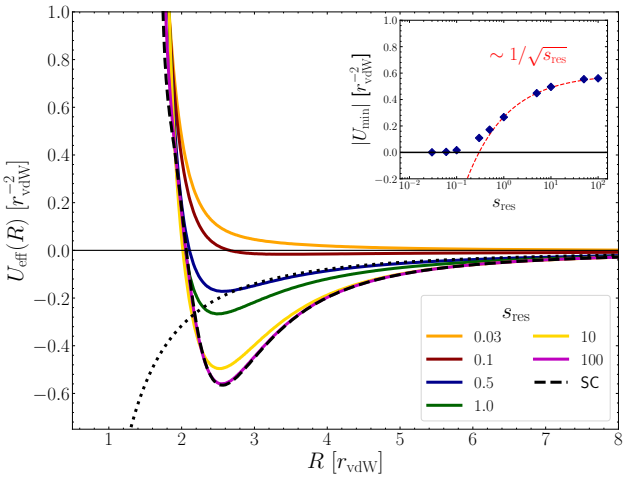

FIG. 7. Plot of the effective three-body potential as a function of the hyperradius, computed with starting parameters taken from the ^{39}K resonance as outlined in table I. Solid coloured lines show the effective potential at different values of the resonance strength parameter. In the regime of small hyperradius $R \lesssim r_{\rm vdW}$ there appear unphysical and meaningless oscillations in the potential as artifacts of the model [13], which we have removed from the plot to avoid unnecessary clutter. Black dashed line shows the effective potential computed by using the associated SC-EST model. The black dotted line shows the asymptotic $\sim 1/R^2$ Efimov attraction as follows from the zero-range theory. Plot includes an inset showing the scaling of the minimum $U_{\rm min}(R)$ with $s_{\rm res}$.

three-body effective potentials for particles interacting via exponentially decaying potentials, common in nuclear physics. Here the three-body parameter is likewise different compared to the single-channel van der Waals interaction, but in contrast to our multichannel results there is a genuine shift in the location of the three-body repulsive barrier. This suggests that the change in three-body potential as observed in Fig. 7 originates from genuine multichannel effects, which we will analyse more in the next section. The analysis of the nuclear potentials can be found in Appendix A.

C. Analysis in spin-position space

To gain better physical understanding of the origin of the observations made in the previous section, it is instructive to consider the multichannel effects on the three-body level in more detail. To this end we generalize our theoretical description and write the open-channel two-body state as $|\underline{aa}\rangle$, where $|a\rangle$ is the lowest single-particle spin state and the underbar denotes symmetrization. A Fesbach resonance is induced by tuning a bound state in an arbitrary closed channel $|\underline{bc}\rangle$ to the scattering threshold, which strongly enhances the effective interac-

tion strength in the $|\underline{aa}\rangle$ channel via the presence of the bound state (see Appendix B).

We consider now the effect of the enhanced interaction at the three-body level. In the pure open channel state $|\underline{aaa}\rangle$, every pair of particles interacts via the strong resonant van der Waals interaction which induces the Efimov effect. Together with the suppression of two-body probability when $r < r_{\rm vdW}$, this will drive the particles towards equilateral three-body configurations in which all nuclear distances are maximized. As mentioned in the previous section, these dynamics are recognized in the hyperspherical picture via the non-adiabatic potential $Q_{00}(R)$, which forms a strong repulsive barrier at small hyperradii [12, 13]. In the multichannel case, the physical picture is complicated by the presence of a closed-channel three-body state $|\underline{bc}a\rangle$. In this state there appears an asymmetry in the strength of the two-particle interactions, given that two of the three pairs exist in the non-resonant channels $|\underline{ab}\rangle$ and $|\underline{ac}\rangle$. Hence the interaction with the third particle is much weaker than the interaction felt by the two particles in the resonant state, altering the resulting dynamics.

With these effects in mind we now turn our attention once more to the results presented in Fig. 7. As we decrease the resonance strength, the lifetime of the closed-channel state increases, scaling as $1/s_{\rm res}$. Consequently the attractive interaction with the third particle weakens, due to the imbalance between the background interactions and the resonant interaction in the $|\underline{aa}a\rangle$ channel. This leads to a gradual decrease of the depth of the effective potential, as the coupling to the closed channel $|\underline{bc}a\rangle$ stretches the three-body state to more elongated configurations. To illustrate this behaviour we have computed the closed-channel component $\langle \underline{bc}a|\bar{\Psi}\rangle$ of the three-body wave function, which in our formalism can be obtained as,

$$\langle kp;\underline{bc}a|\bar{\Psi}\rangle = -\frac{F(\kappa,p)g_2(k)}{\kappa^2+\varepsilon_{\rm c}(B)+k^2+\frac{3}{4}p^2}, \qquad (27)$$

where we have inserted the closed-channel form factor $g_2(k)$. From this expression we derive the closed-channel three-body probability $P_{\underline{bc}a}$, plotted in Fig. 8. Here one clearly observes the stretching of the wave function that occurs near a narrow resonance, which is directed along the ρ coordinate quantifying the separation of the third particle. In the limit of a very narrow resonance, the third particle is free to drift towards separations far beyond $r_{\rm vdW}$, consistent with a flat three-body potential. In contrast the shape of the probability along the dimer separation r is relatively unaffected by the resonance strength, and in fact follows the structure of the two-body closed channel wave function as shown in Fig. 5. Fig. 8 also shows that there is no repulsive barrier at small hyperradii in the closed channel state, which as discussed above is due to the asymmetry between the interaction strengths at the two-particle level. The fact that a universal short-range repulsive barrier still remains also for narrow resonances is due to the influence of the

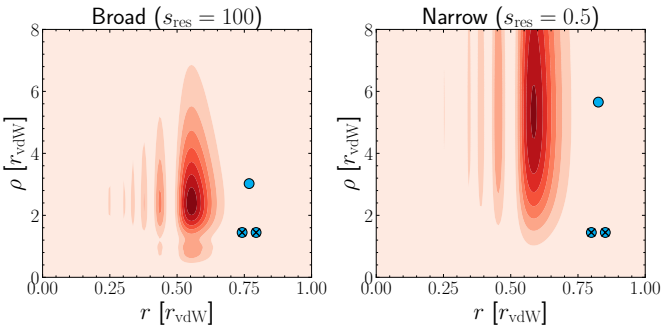

FIG. 8. Contour plots of three-body probability $P_{\underline{bc}a}(r,\rho) \sim r^2\rho^2 |\langle r\rho;\underline{bc}a|\Psi\rangle|^2$ in the plane of Jacobi coordinates r and ρ, for a broad and narrow Feshbach resonance. Note that $\langle \underline{bc}a|\Psi\rangle = \langle \underline{bc}a|\bar{\Psi}\rangle$ since $\langle \underline{abc}|\bar{\Psi}\rangle$ and $\langle \underline{acb}|\bar{\Psi}\rangle$ vanish in the ESC Faddeev equations by the absence of background interactions [18]. The drawings show the changing structure of the Efimov state, where particles in the closed channel $|\underline{bc}\rangle$ are drawn with a cross.

open-channel component, where a universal barrier due to $Q_{00}(R)$ always exists and is independent of resonance strength. This prevents coupling to the closed-channel state for small hyperradii, hence preserving the short-range suppression of the wave function, as clearly observed in Figs. 6 and 7.

As a final note we comment that the relative unimportance of the background interactions is actually an underlying assumption in the ESC model of the three-body problem. As discussed in detail in Ref. [18], Eq. (19) is obtained by taking the limit in which interactions in the non-resonant channels $|\underline{ab}\rangle$ and $|\underline{ac}\rangle$ are turned off completely. While this is a valid assumption for most practical systems as we have argued above, there are special cases where such an approach is expected to be incorrect. For example, if the resonant closed channel state is taken as $|\underline{ab}\rangle$, i.e. just one particle changes its state, then both the open and closed channel three-body states have purely resonant interactions. We can expect this to alter the behaviour of the three-body potential, and indeed it was shown in Ref. [18] that for closed channels of this type the scaling of the three-body parameter with $s_{\rm res}$ is actually inverted.

V. CONCLUSION AND OUTLOOK

In this work we have analysed the change in the Efimovian three-body potential as the Feshbach resonance strength is tuned from the broad to narrow resonance regime. For this purpose we have developed a two-channel separable model that takes into account the full coupled-channels low-energy scattering wave function. Our numerical results show that as the resonance strength is tuned away from the broad limit, the associated change in the three-body parameter a_- originates from a decrease of the three-body potential depth in the

intermediate distance regime where $R > 2\ r_{\rm vdW}$. In contrast, the three-body repulsive barrier that is observed in single-channel models at $R \approx 2\ r_{\rm vdW}$ remains universally determined by the van der Waals length. We have interpreted our observations to originate from the relative weakness of background interactions between non-resonant spin-channels compared to the resonant interaction that exists in the open channel and drives the Efimov effect. Hence our results should apply generally to systems in which the Feshbach resonance is sufficiently isolated.

There are several possible opportunities for extensions of our approach. Our physical picture of the decreasing three-body attraction for narrow resonances rests on the assumption that the interaction between closed and open-channel particles is off-resonant, such that it may be neglected. Consequently we expect that the presence of a resonant third-channel alters the behaviour of the potential significantly, which could be accurately captured in a three-channel EST model. Another point of interest is the analysis of special closed-channel configurations of the type $|\underline{ab}\rangle$, where it is known that the value of $|a_-|$ decreases for a narrow resonance [18]. Such a system however is not easily analysed with our model, since the trimer wave function becomes more localised in the short-range where the effective three-body potential is not a useful construct.

ACKNOWLEDGMENTS

We thank Pascal Naidon and Thomas Secker for discussions. This research is financially supported by the Dutch Ministry of Economic Affairs and Climate Policy (EZK), as part of the Quantum Delta NL programme, and by the Netherlands Organisation for Scientific Research (NWO) under Grant No. 680-47-623.

Appendix A: Comparison with nuclear interactions

In Sec. IV C we argue that our observations in the multichannel model arise due to a distinct interplay between the different possible spin-states on the three-body level. It is known however that the value of $|a_-|$ can also increase with different kinds of asymptotic three-body interactions, without any need for additional spin-channels. In this appendix we contrast the changing three-body potential in systems of this type with our previous multichannel results, to show that the underlying mechanisms are indeed fundamentally different. Specifically we will consider single-channel EST models based on two-body interactions that decay exponentially in the long range, common in nuclear physics. For this class of interactions the short-range two-body suppression looks rather different from the van der Waals potential, where "short-range" is now interpreted as $r < r_e/2$, with r_e the effective range constant. To illustrate the differences we plot

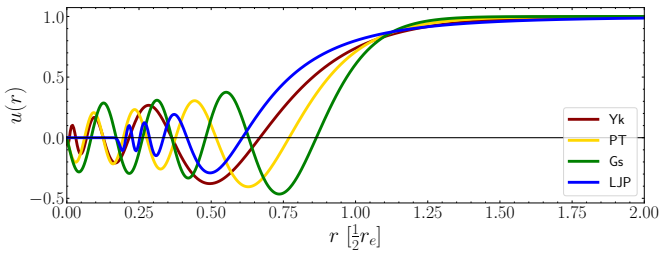

FIG. 9. Two-body radial wave functions at the appearance of the eighth potential resonance of the three nuclear interactions in Eq. (A1) and the LJP van der Waals interaction in Eq. (2). All distances have been expressed in the associated effective range scale $r_e/2$.

in Fig. 9 the two-body wave function at unitarity for the following set of nuclear potentials,

$$\begin{aligned} V_{\rm PT} &\sim -\eta \cosh^{-2}(r)\,, \\ V_{\rm Yk} &\sim -\frac{\eta}{r}\exp(-r)\,, \\ V_{\rm Gs} &\sim -\eta \exp\left(-r^2\right), \end{aligned} \tag{A1}$$

which respectively are the usual Pöschl-Teller (PT), Yukawa (Yk), and Gaussian (Gs) potentials [12, 31]. The strength parameter η is used to tune the potential towards resonance. Similar to the case of van der Waals interactions, the short-range suppression in the two-body wave function leads to the formation of a three-body repulsive barrier and hence a universal value for the three-body parameter in the limit of broad Feshbach resonances. As was shown in Ref. [31], this universal value matches the three-body parameter that one obtains when using a simple step function as input into the EST model, which is zero for $r < r_e/2$ and unity everywhere else. Indeed for an infinite number of two-body bound states the PT, Yk and Gs wave functions in Fig. 9, will all approach step functions [31]. This is not the case for the LJP interaction, whose infinitely deep limit is obtained by taking $r_0 \to 0$, yielding a pure (but ill-behaved) van der Waals potential. Interesting for this work is the fact that the three-body parameter $|a_-|$ obtained from the step-function limit in a single-channel model is ~ 19 % *larger* than the value obtained from the van der Waals interaction [31]. In our multichannel model we similarly observe an increased value of $|a_-|$ when $s_{\rm res}$ is decreased away from the broad resonance limit. Evidently however the associated change in the two-body wave function is very different, as becomes clear when comparing Figs. 5 and 9. Whereas in the multichannel model the open-channel component that underlies the Efimov state was unchanged, for the interactions in this section there is a clear change in the short-range suppression in the open-channel. As shown in Fig. 10, this subsequently leads to a shift in the location of the three-body barrier, which is absent in the multichannel model as explained in Sec. IV C.

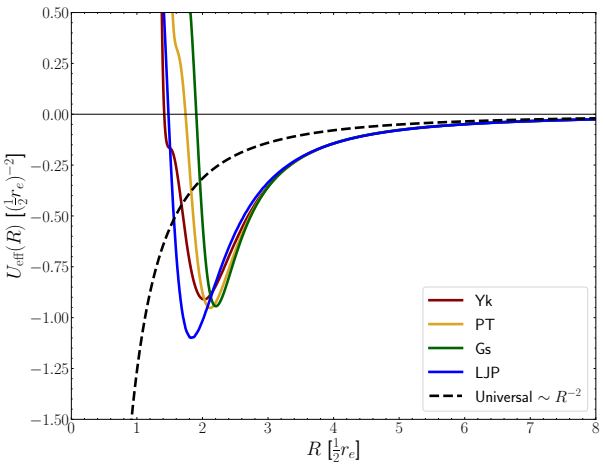

FIG. 10. Plot of the effective three-body potential as a function of the hyperradius, in units of the effective range. Solid coloured lines show the effective potential for different shapes of the two-body interaction, tuned to a depth of eight dimer states. The black dotted line shows the asymptotic $\sim 1/R^2$ Efimov attraction as follows from the zero-range theory.

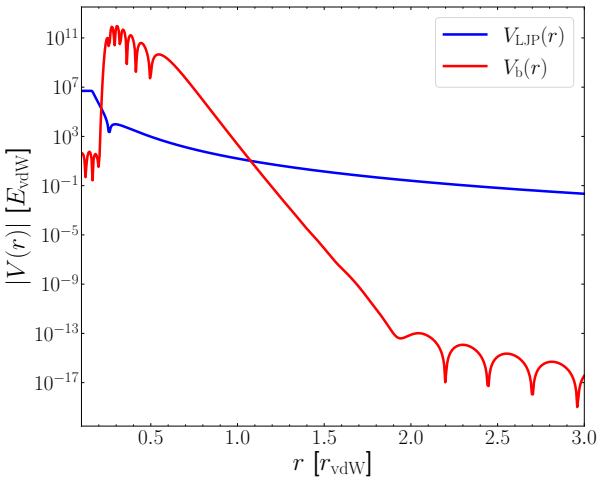

FIG. 11. Comparison of the absolute magnitudes of the EST potential $V_b(r)$ associated with the closed-channel bound state, and the background van der Waals interaction $V(r)$, as a function of the particle separation. Note that for $V_b(r)$ the diagonal elements of the non-local potential matrix are plotted.

Appendix B: Comparison of resonant to background interactions

In Sec. IV C we argue that the interaction in the open channel $|\underline{aa}\rangle$ will dominate any background interactions in other channels due to the enhanced coupling to a near-threshold bound state in the closed channel. To quantify this effect more precisely we can compute an EST potential associated with the closed channel bound state $|\varphi\rangle$, given as $V_{\rm b} = V|\varphi\rangle\langle\varphi|V|\varphi\rangle^{-1}\langle\varphi|V$. This potential may be interpreted as an effective potential for the bound state which we use to quantify the strength of the two-body interaction. In Fig. 11 we plot the magnitude of $\langle\mathbf{r}|V_{\rm b}|\mathbf{r}\rangle$ compared to the LJP potential that quantifies a background van der Waals interaction. One clearly observes that the effective interaction in the closed channel can augment the background interaction by several orders of magnitude, which supports our physical picture.

Appendix C: Analysis of a physical resonance

Since the ESC-EST model can take any arbitrary multichannel interaction as input, we can also perform a more detailed analysis of a specific physical resonance. To test such an approach we have analysed the ^{39}K resonance as summarised in table I, using the Born-Oppenheimer corrected molecular interaction formulated in Ref. [46] as input. This resonance has recently received some interest in the literature since experimental data of the three-body parameter has revealed a significant shift away from the universal value [11, 30]. With our model we extract a value $a_- = -13.56\ r_{\rm vdW}$, which

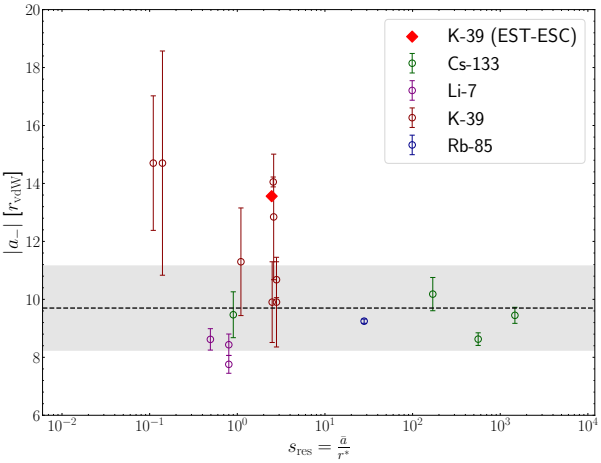

FIG. 12. Plot of experimentally measured three-body parameter $|a_-|$ for different atomic species, set out against the strength of the associated Feshbach resonance. Dark red diamond shows the result obtained with the ESC-EST model using the molecular potential of [46] as input.

indeed falls outside the van der Waals universal region. In Fig. 12 we show our result amongst the set of experimental results also presented in Fig. 4. Evidently the ESC-EST model produces a three-body parameter that is consistent with the current experimental data, and in particular falls within the uncertainty interval of the result of Ref. [11]. We should note however that the data for potassium is also consistent with our more approximate van der Waals model presented in the main text, so we can at present not say whether the accuracy of this method will extend to other atomic species as well. The lithium data for example suggests a downward trend

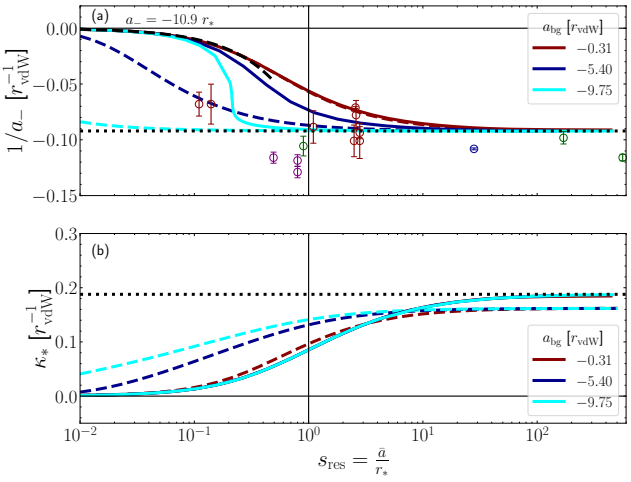

FIG. 13. Comparison of the three-body parameter a_- in Fig. (a) and κ_* in Fig. (b) as a function of the resonance strength for the ESC-EST model shown with solid coloured lines, and the cut-off form factor model shown with dashed coloured lines. The experimental data shown before in Fig. 4 is also included. Both figures show the SC-EST result with a black dotted line, correspondent with the broad resonance limit for the EST interaction. Note that the solid lines for κ_* practically overlap.

of the three-body parameter, which has not been seen in any of our test cases and would likely require a more fundamental change in our approach, as was also mentioned in Sec. IV A.

Appendix D: Comparison of EST approach with a momentum cutoff

As mentioned in section IV our results show a significant decrease in sensitivity to the background scattering length compared to simpler models of the interaction. To test this observation we have performed computations with a different and much less complex separable potential, defined as,

$$\tilde{V} = \frac{\hbar^2}{m\Lambda} \begin{pmatrix} \lambda_{oo} & \lambda_{oc} \\ \lambda_{co} & \lambda_{cc} \end{pmatrix} |g\rangle \langle g| \,. \tag{D1}$$

The momentum Λ defines a cut-off scale for the form factors

$$g(k) = \begin{cases} 1 & k < \Lambda \\ 0 & k \geq \Lambda \end{cases} . \tag{D2}$$

This model reduces to a contact interaction in the limit $\Lambda \to \infty$, such that the scale Λ^{-1} acts analogous to the range of the potential. Using the techniques of Feshbach resonance theory one can derive a mapping from the input resonance parameters a_{bg} and r_* to appropriate values of the $\lambda_{oo/oc/co/cc}$ coefficients. This model has been taken directly from Ref. [18], and we refer the reader to this paper for more details of this approach. In Fig. 13 we show a comparison between the three-body parameter as obtained for negative scattering lengths presented in Fig. 4(a), and the results we obtain with this model.

To present the results in van der Waals units we have rescaled the broad resonant universal value of $|a_-|$ in the cut-off model to match that of the ESC-EST model. Because the two models produce different ground state ratios $\kappa_*|a_-|$, this choice leads to a slightly different value of the universal κ_* value for both models. What we want to emphasize here is the significant reduction in the sensitivity to the background scattering length that we find with our more realistic EST separable potential compared to the much simpler model with a cut-off form factor.

[1] V. Efimov, Phys. Lett. B **33**, 563 (1970).
[2] V. Efimov, Sov. J. Nucl. Phys. **12**, 589 (1971).
[3] B. D. Esry, C. H. Greene, and J. P. Burke, Phys. Rev. Lett. **83**, 1751 (1999).
[4] T. Kraemer, M. Mark, P. Waldburger, J. G. Danzl, C. Chin, B. Engeser, A. D. Lange, K. Pilch, A. Jaakkola, H.-C. Nägerl, and R. Grimm, Nature **440**, 315 (2006).
[5] E. Braaten and H.-W. Hammer, Physics Reports **428**, 259 (2006).
[6] P. Naidon and S. Endo, Rep. Prog. Phys. **80**, 056001 (2017).
[7] M. Berninger, A. Zenesini, B. Huang, W. Harm, H.-C. Nägerl, F. Ferlaino, R. Grimm, P. S. Julienne, and J. M. Hutson, Phys. Rev. Lett. **107**, 120401 (2011).
[8] N. Gross, Z. Shotan, O. Machtey, S. Kokkelmans, and L. Khaykovich, C. R. Phys. **12**, 4 (2011).
[9] P. Dyke, S. E. Pollack, and R. G. Hulet, Phys. Rev. A **88**, 023625 (2013).
[10] R. J. Wild, P. Makotyn, J. M. Pino, E. A. Cornell, and D. S. Jin, Phys. Rev. Lett. **108**, 145305 (2012).
[11] R. Chapurin, X. Xie, M. J. Van de Graaff, J. S. Popowski, J. P. D'Incao, P. S. Julienne, J. Ye, and E. A. Cornell, Phys. Rev. Lett. **123**, 233402 (2019).
[12] J. Wang, J. P. D'Incao, B. D. Esry, and C. H. Greene, Phys. Rev. Lett. **108**, 263001 (2012).
[13] P. Naidon, S. Endo, and M. Ueda, Phys. Rev. A **90**, 022106 (2014).
[14] C. Chin, R. Grimm, P. Julienne, and E. Tiesinga, Rev. Mod. Phys. **82**, 1225 (2010).
[15] G. F. Gribakin and V. V. Flambaum, Phys. Rev. A **48**, 546 (1993).
[16] D. S. Petrov, Phys. Rev. Lett. **93**, 143201 (2004).

[17] Y. Nishida, Phys. Rev. Lett. **109**, 240401 (2012).
[18] T. Secker, D. J. M. Ahmed-Braun, P. M. A. Mestrom, and S. J. J. M. F. Kokkelmans, Phys. Rev. A **103**, 052805 (2021).
[19] F. H. Mies, E. Tiesinga, and P. S. Julienne, Phys. Rev. A **61**, 022721 (2000).
[20] N. Nygaard, B. I. Schneider, and P. S. Julienne, Phys. Rev. A **73**, 042705 (2006).
[21] Y. Wang and P. Julienne, Nat. Phys. **10**, 768–773 (2014).
[22] The advantage of using the r^{-10} core instead of the more traditional r^{-12} shape is the fact that the associated zero-energy scattering problem allows for an exact solution in terms of hyperconfluent geometric functions. Thus the length scale σ can be analytically related to the scattering length, making it straightforward to fix a_{bg}. This interaction was characterised by J. Pade, cited in the next reference.
[23] J. Pade, Eur. Phys. J. D **44**, 345 (2007).
[24] This value was chosen for approximate correspondence with the coupling in the realistic multichannel ^{39}K potential as used in Appendix C. As expected our results are largely insensitive to changes in r_W, since they are compensated by a corresponding change in β, with the caveat that r_W should remain significantly smaller than r_{vdW}.
[25] C. H. Greene, A. R. P. Rau, and U. Fano, Phys. Rev. A **26**, 2441 (1982).
[26] F. H. Mies, J. Chem. Phys. **80**, 2514 (1984).
[27] F. H. Mies and P. S. Julienne, J. Chem. Phys. **80**, 2526 (1984).
[28] K. Jachymski and P. S. Julienne, Phys. Rev. A **88**, 052701 (2013).
[29] P. Naidon and L. Pricoupenko, Phys. Rev. A **100**, 042710 (2019).
[30] T. Secker, J.-L. Li, P. M. A. Mestrom, and S. J. J. M. F. Kokkelmans, Phys. Rev. A **103**, 022825 (2021).
[31] P. Naidon, S. Endo, and M. Ueda, Phys. Rev. Lett. **112**, 105301 (2014).
[32] D. Ernst, C. Shakin, and R. Thaler, Phys. Rev. C **8**, 46 (1973).
[33] J. Taylor, *Scattering Theory: The Quantum Theory of Nonrelativistic Collisions*, 1st ed. (Dover Publications, Inc., 2006).
[34] T. Karman, L. M. C. Janssen, R. Sprenkels, and G. C. Groenenboom, J. Chem. Phys. **141**, 064102 (2014).
[35] K. Willner, O. Dulieu, and F. Masnou-Seeuws, J. Chem. Phys. **120**, 548 (2004).
[36] T. Secker, J.-L. Li, P. M. A. Mestrom, and S. J. J. M. F. Kokkelmans, Phys. Rev. A **103**, 032817 (2021).
[37] L. Faddeev, Sov. Phys. JETP **12**, 1014 (1961).
[38] W. Glöckle, *The quantum mechanical few-body problem*, Texts and monographs in physics (Springer, Berlin, 1983).
[39] J. J. Sakurai and J. Napolitano, *Modern Quantum Mechanics*, 2nd ed. (Cambridge University Press, 2017).
[40] J.-L. Li, X.-J. Hu, Y.-C. Han, and S.-L. Cong, Phys. Rev. A **94**, 032705 (2016).
[41] G. V. Skorniakov and K. A. Ter-Martirosian, Soviet Phys. JETP **31**, 775 (1957).
[42] J. Macek, J. Phys. B: Atom. Mol. Phys. **1**, 831 (1968).
[43] J. Macek, Z. Phys. B **3**, 31 (1986).
[44] E. Nielsen, D. Fedorov, A. Jensen, and E. Garrido, Phys. Rep. **347**, 373 (2001).
[45] E. Braaten, H.-W. Hammer, and M. Kusunoki, Phys. Rev. A **67**, 022505 (2003).
[46] S. Falke, H. Knöckel, J. Friebe, M. Riedmann, E. Tiemann, and C. Lisdat, Phys. Rev. A **78**, 012503 (2008).
[47] N. R. Claussen, S. J. J. M. F. Kokkelmans, S. T. Thompson, E. A. Donley, E. Hodby, and C. E. Wieman, Phys. Rev. A **67**, 060701 (2003).
[48] A. Derevianko, W. R. Johnson, M. S. Safronova, and J. F. Babb, Phys. Rev. Lett. **82**, 3589 (1999).
[49] M. Berninger, A. Zenesini, B. Huang, W. Harm, H.-C. Nägerl, F. Ferlaino, R. Grimm, P. S. Julienne, and J. M. Hutson, Phys. Rev. A **87**, 032517 (2013).
[50] C. Langmack, R. Schmidt, and W. Zwerger, Phys. Rev. A **97**, 033623 (2018).
[51] R. Schmidt, R. Rath, and W. Zwerger, Eur. Phys. J. B **85**, 386 (2012).
[52] P. K. Sørensen, D. V. Fedorov, A. S. Jensen, and N. T. Zinner, Phys. Rev. A **86**, 052516 (2012).
[53] B. Gao, Phys. Rev. A **84**, 022706 (2011).
[54] S. Roy, M. Landini, A. Trenkwalder, G. Semeghini, G. Spagnolli, A. Simoni, M. Fattori, M. Inguscio, and G. Modugno, Phys. Rev. Lett. **111**, 053202 (2013).
[55] T. Köhler, K. Góral, and P. S. Julienne, Rev. Mod. Phys. **78**, 1311 (2006).